

ModeDreamer: Mode Guiding Score Distillation for Text-to-3D Generation using Reference Image Prompts

Uy Dieu Tran^{1*} Minh Luu^{1*}
Phong Nguyen¹ Khoi Nguyen¹ Binh-Son Hua²

¹VinAI Research, Vietnam ²Trinity College Dublin, Ireland

{v.uytd,v.minhlnh,v.phongnh31,v.khoindm}@vinai.io binhson.hua@tcd.ie

Abstract

Existing Score Distillation Sampling (SDS)-based methods have driven significant progress in text-to-3D generation. However, 3D models produced by SDS-based methods tend to exhibit over-smoothing and low-quality outputs. These issues arise from the mode-seeking behavior of current methods, where the scores used to update the model oscillate between multiple modes, resulting in unstable optimization and diminished output quality. To address this problem, we introduce a novel image prompt score distillation loss named ISD, which employs a reference image to direct text-to-3D optimization toward a specific mode. Our ISD loss can be implemented by using IP-Adapter, a lightweight adapter for integrating image prompt capability to a text-to-image diffusion model, as a mode-selection module. A variant of this adapter, when not being prompted by a reference image, can serve as an efficient control variate to reduce variance in score estimates, thereby enhancing both output quality and optimization stability. Our experiments demonstrate that the ISD loss consistently achieves visually coherent, high-quality outputs and improves optimization speed compared to prior text-to-3D methods, as demonstrated through both qualitative and quantitative evaluations on the T3Bench benchmark suite.

1. Introduction

The generation of 3D assets continues to be a dynamic and influential research field within computer vision and computer graphics, driven by diverse applications in gaming, film, e-commerce, and robotics. High-quality 3D content creation is resource-intensive, making automated 3D generation a key research objective. Recent advancements in neural scene representations [19, 36] and diffusion-based

generative models [7, 41] have led to significant progress in producing creative 3D content from text prompts [38, 53].

To generate a 3D model from a text prompt, a notable approach is to optimize a 3D representation using distillation-based method, which utilizes a pretrained text-to-image diffusion model to guide the generation of 3D objects. Since DreamFusion [38], SDS-based methods [32, 39, 39, 53] offer superior 3D generation quality, albeit being more expensive in its optimization to generate 3D models. These methods have been designed to address the limitations of the original SDS, mitigating over-smoothing and over-saturation effects.

At its core, score distillation sampling aims to optimize the KL-divergence between the Gaussian distributions in a forward diffusion process and the distribution of a pretrained diffusion model [38]. One challenge in this optimization process is the mode-seeking behavior of the KL-divergence, which is difficult to control and has limited capability to produce diverse and high-quality 3D objects. Some previous methods attempted to address the limitations of SDS loss by employing variational score distillation (VSD) [53], reducing gradient variance [27], or utilizing two-stage training strategies [3, 24, 35]. Furthermore, according to the leaderboards from T3bench [11] and GPTEval3D [56], the quality of 3D objects generated by VSD remains superior, despite significantly slow generation time.

In this paper, we address such mode-seeking issues by directly guiding mode convergence using image prompts during score distillation sampling. Our idea is to view the text-to-image diffusion prior as an integral of conditional distributions conditioned on reference image prompts. This conceptual change allows us to use a reference image to directly guide score distillation sampling to converge to a favorable mode specified in the reference, thereby resolving the ambiguity faced in mode seeking. We design our method based on IP-Adapter [61], a lightweight adapter for pretrained text-to-image diffusion models to integrate guid-

*First two authors contribute equally.

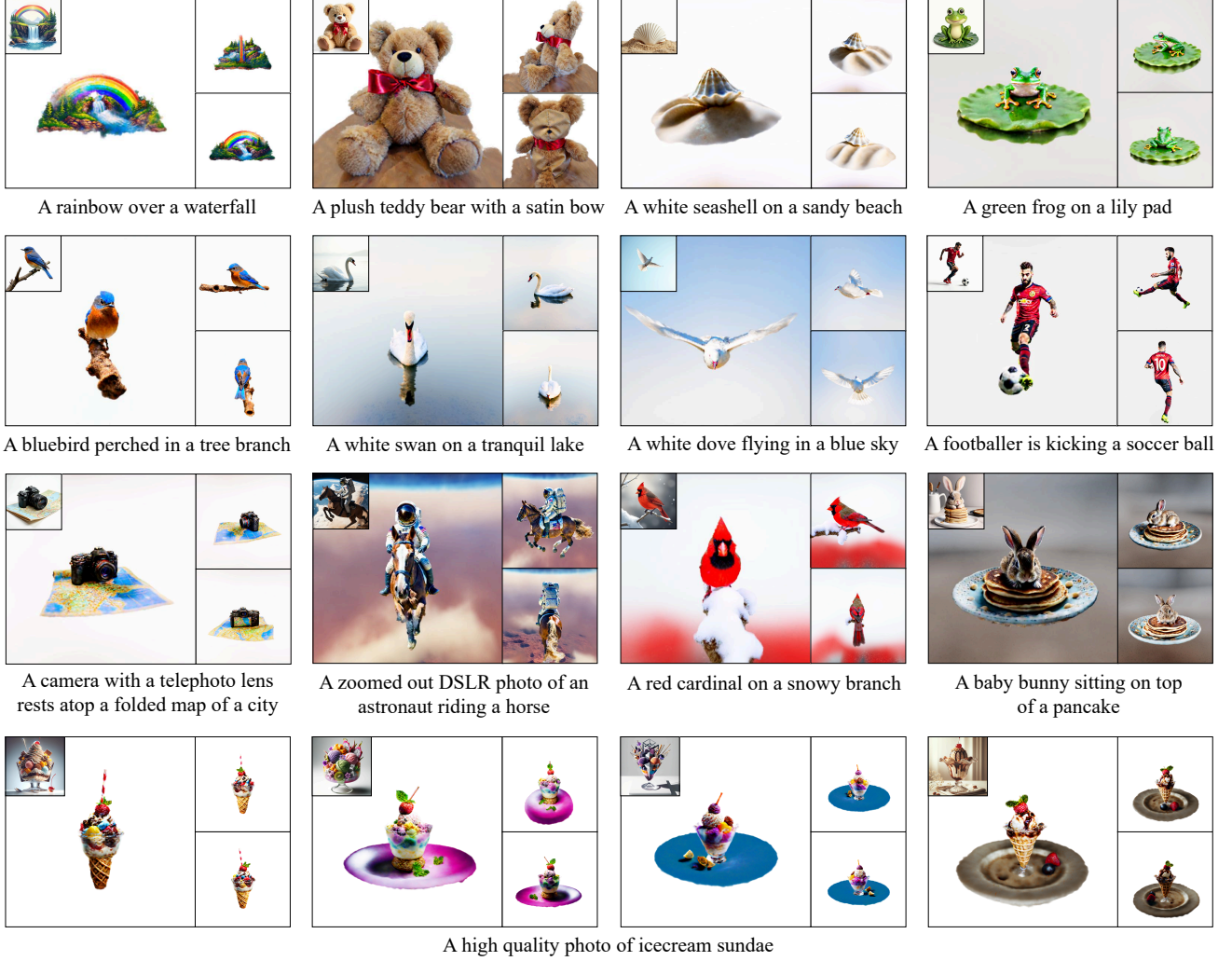


Figure 1. Our mode-guiding score distillation using the ISD loss explicitly selects a desired mode captured in a diffusion prior using a reference image prompt to steer text-to-3D generation. Our method leads to high-quality and diverse 3D generation. For each sub-figure, the top-left illustrates the reference image used for mode selection, and the remaining images illustrate different views of the generated object. The last row demonstrates the diversity of our 3D generation by using different reference images on the same text prompt.

ance from image prompts. By exploiting the positive correlation between the noise prediction by the diffusion prior with and without a reference image prompt, respectively, we devise *Image prompt Score Distillation (ISD)*, a novel distillation with lower variance in its score estimates due to a more effective control variate based on our adapter. This strategy enables us to effectively steer and control the score distillation process, resulting in diverse high-quality 3D outputs that capture the variability and fidelity of the reference images. To mitigate the multi-face Janus artifact, we combine the advantages of our proposed ISD loss with an enhanced SDS variant that incorporates a multi-view diffusion prior, such as MVDream [46] or Zero123 [28, 45]. This integration promotes cross-view consistency and significantly enhances the overall quality of the 3D outputs.

We evaluate our method on the recently introduced T3Bench [10], a text-to-3D benchmark containing diverse text prompts across three complexity levels, specifically designed for the 3D generation task, and compare it with state-of-the-art text-to-3D score distillation methods. Both qualitative and quantitative results demonstrate the effectiveness of our approach over previous methods. Our method produces 3D assets with realistic appearance and shape, and is capable of generating a diverse range of 3D objects from the same text prompt, as demonstrated in Fig. 1. In summary, our main contributions are as follows:

- We analyze the mode-seeking behavior of the SDS loss and propose to leverage the visual prompting capabilities of IP-Adapter [61] to effectively guide and stabilize the

noisy score distillation for text-to-3D generation.

- We introduce a novel variate control term in score distillation, which reduces variance in score estimates. We achieve high-quality 3D generation without the need of LoRA training in an alternative optimization fashion as done in previous methods like VSD [53].
- Our method achieves high-quality and diverse 3D results comparable to state-of-the-art approaches [32, 33, 39], with the added advantage of significantly reduced optimization time, requiring only 30-40 minutes compared to the several hours of training needed by VSD [53].

2. Related Work

Text-to-Image Generation. Early text-to-image generation extended GAN architectures [8] to condition on textual inputs by mapping text embeddings into the image space, but these faced challenges with training stability and limited diversity due to mode collapse. Diffusion models [1, 40–42, 63] significantly advanced the field by leveraging large image-text pair datasets for modeling the relationships between text and images distribution through iterative denoising processes, offering higher image quality, diversity, and improved stability over GANs. IP-Adapter [61] further enhanced alignment with user intent through a decoupled cross-attention mechanism incorporating both text and image inputs. Our approach builds on IP-Adapter by additionally conditioning on a reference image.

Image/Text-to-Multiview Synthesis. Consistent multi-view image generation is crucial for many applications. Several methods [28, 45, 52] can generate novel views from an input image by fine-tuning pretrained text-to-image models on large-scale 3D datasets [4, 5], accounting for camera positions. These methods model view-dependent effects and occlusions to ensure coherence across multiple viewpoints. Text-to-multiview methods like MVDream [46] extend text-to-image generation to multi-view synthesis by fine-tuning pretrained Stable Diffusion with a 3D-aware generative module on 3D data. Our method leverages multi-view prior of MVDream to mitigate the Janus problem.

Image-to-3D Generation. Recent approaches reconstruct 3D models from a single input image using pre-trained diffusion models [12, 23, 26, 29, 34, 44, 47, 49, 54, 55, 59, 66]. These models can generate 3D objects within seconds from real or synthesized images without per-prompt optimization, significantly reducing computational demands compared to traditional techniques. Despite their impressive results, they struggle with complex scenes involving intricate geometries or textures, especially thin structures, leading to reduced detail or incomplete reconstructions. Additionally, they heavily rely on large-scale 3D datasets [4, 5] for training, but since these datasets are smaller than image-text datasets like LAION-5B [43], the models have limited



Figure 2. Comparison between vanilla SDS and IP-SDS, IP-SDS can generate detail and sharp texture while original SDS cannot.

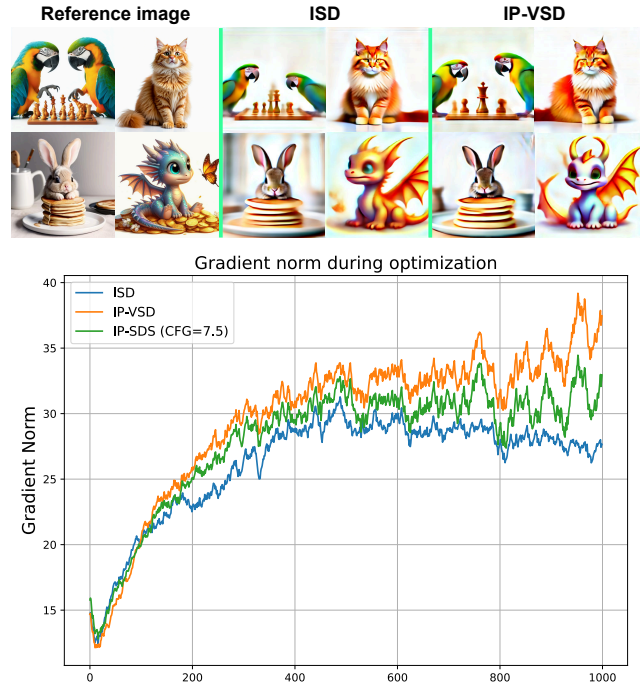


Figure 3. A 2D toy experiment. Our ISD can generate results similar to IP-VSD while having lower gradient variance. This advocates designing better control variates, discarding the need of training LoRA in an alternative fashion like in VSD.

generalization to unseen objects and struggle with images containing multiple objects or complex lighting conditions and backgrounds.

Text-to-3D Generation. Training-based methods [22, 39, 47, 57] learn a direct mapping from text to 3D representations through supervised learning on large 3D datasets [4, 5], but require extensive annotated data and significant computational resources. In contrast, optimization-based methods iteratively optimize a 3D representation to align with a text prompt, guided by pretrained text-to-image models. Foundational approaches [15, 38] use pretrained diffusion

models to guide the optimization of neural radiance fields (NeRFs)[36] by minimizing the difference between rendered images and the target distribution conditioned on the prompt. However, generating a 3D model for each prompt is resource-intensive. To address this, Lorraine et al. [30] propose an amortized optimization approach by training a unified model on multiple prompts simultaneously. This approach shares computation across prompts, reducing training time compared to per-prompt optimization. Other approaches focus on improving the visual quality and fidelity of generated 3D models [2, 3, 6, 14, 16, 18, 20, 32, 33, 39, 53, 65] or computational intensity [48, 62] by utilizing more efficient 3D representations, such as Gaussian Splatting [19]. Some tackle mode collapse in SDS loss [50, 60], enabling diverse 3D content generation from the same text. For example, DiverseDream [50] encourages the exploration of multiple plausible solutions to generate diverse outputs from a single text prompt. VP3D [3] employs an image-conditioned diffusion model to supervise the creation of 3D models, with multiview regularization being novel views synthesized from Zero123 [28]. This approach may lead to inconsistent 3D results due to two primary factors: 1) the inherent inconsistencies of Zero123 [28] and 2) the underperformance of the image-conditioned diffusion model in novel view conditioning. Our approach, using ISD loss, further mitigates the mode-seeking behavior of the SDS by leveraging guidance from reference images while ensuring consistent views of 3D objects.

3. Background and Analysis

To generate coherent 3D objects without direct 3D data, the priors of a Latent Diffusion Model (LDM) can be leveraged to guide the creation of standard 3D representations, such as NeRF [36] or 3D Gaussian splatting [19]. Specifically, a 3D representation parameterized by θ is iteratively optimized to align its rendered images $x = g(\theta, c)$ with LDM’s distribution given a text prompt y .

3.1. Score distillation sampling (SDS)

DreamFusion [38] proposed SDS loss to generate 3D models. The loss is formulated as:

$$\text{KL}(q(z_t|x = g(\theta, c))||p_\phi(z_t|y)), \quad (1)$$

where $q(z_t|x = g(\theta, c))$ is a Gaussian distribution representing a forward diffusion process of the rendered images, and $p_\phi(z_t|y)$ denoting the marginal distribution at timestep t of a pretrained LDM model. The gradient is calculated as:

$$\nabla_\theta \mathcal{L}_{\text{SDS}} \triangleq \mathbb{E}_{t, \epsilon, c} \left[\omega(t) (\epsilon_\phi(x_t, t, y) - \epsilon) \frac{\partial g(\theta, c)}{\partial \theta} \right], \quad (2)$$

where $\omega(t)$ is a time-dependent weighting function, $\epsilon_\phi(\cdot)$ is the predicted noise of LDM given the noisy input image

$x_t = \alpha_t x + \sigma_t \epsilon$ created by adding Gaussian noise ϵ to the rendered image x at timestep t with noise scheduling coefficients α_t, σ_t . Derived from the reverse KL divergence in Eq. (1), the SDS loss exhibits mode-seeking behavior, aligning a single-mode Gaussian distribution with the complex, multimodal distribution of a pretrained LDM. This leads to oversaturated, oversmoothed, and low-diversity 3D models, as empirically analyzed in [38].

Several enhancements have been introduced to address challenges with the SDS loss. ProlificDreamer [53] improves output quality by replacing the noise term in SDS with adaptive, trainable LoRA [13] layers, which more effectively approximate 3D model scores. Although ProlificDreamer produces high-quality 3D results, it suffers from slow training speeds and instability due to the sensitivity of the LoRA layers.

Other methods, such as ScaleDreamer [33] and CSD [64], aim to accelerate training by approximating LoRA [13] layers using U-Net architectures with varying timesteps or by using only the CFG term in the distillation gradient. While they improve training efficiency, their 3D outputs often show oversaturation. Multi-stage strategies like Magic3D [24], Fantasia3D [2], and Latent NeRF [35] enhance SDS by first training coarse geometry before optimizing texture. However, these methods still encounter issues with over-smoothness, over-saturation, and limited diversity due to reliance on SDS loss. DiverseDream [50] improves 3D output diversity using textual inversion from reference images. However, it struggles with asymmetric object generation and the Janus problem due to bias toward reference views in visual prompts.

3.2. Mode analysis

We hypothesize that the limitations of SDS loss come from oscillations in the modes. As the model samples noise differently at each iteration, the score updates may direct the model toward various modes within the data distribution. Consequently, the resulting 3D models may fail to converge to a single, stable mode. We speculate that if a high-quality mode can be identified in advance, the SDS loss is capable of generating high-quality samples. More specifically, we can express the marginal distribution of the LDM prior $p_\phi(z_t|y)$ by integrating over reference images:

$$p_\phi(z_t|y) = \int_{x_{\text{ref}}} p_\phi(z_t|y, x_{\text{ref}}) p(x_{\text{ref}}|y) dx_{\text{ref}}, \quad (3)$$

where x_{ref} denotes the reference image, $p_\phi(z_t|y, x_{\text{ref}})$ represents the LDM prior conditioned on the additional reference image along with text prompt y , and $p(x_{\text{ref}}|y)$ stands for the distribution of the reference image given a text prompt y . The Eq. (3) suggests that $p_\phi(z_t|y)$ is a combination of multiple modes, which complicates the optimization of the SDS loss. Since x_{ref} provides concrete visual information, the

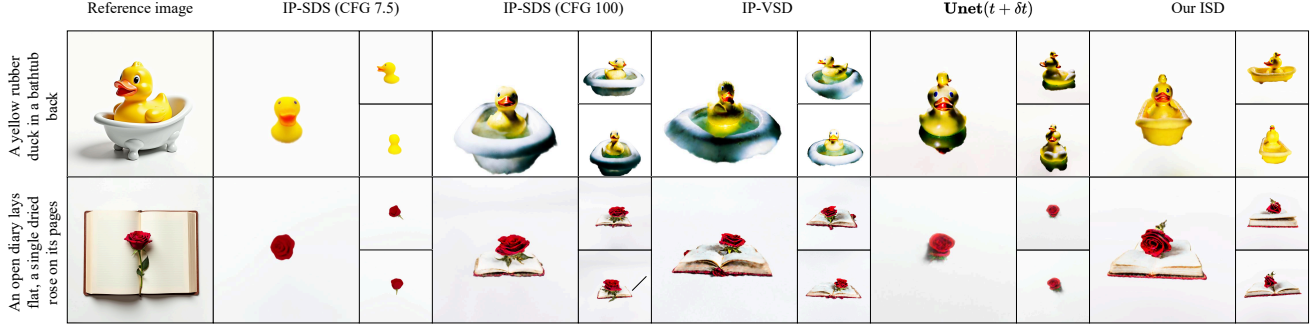


Figure 4. Different control variate settings including Gaussian noise ϵ , learning LoRA-Unet in VSD [53], Unet at different timestep in ScaleDreamer [33], and our ISD. Our method can generate 3D objects on par with VSD without learning additional LoRA-Unet.

model is less likely to oscillate between modes. Instead, it focuses on refining its output around the mode suggested by x_{ref} , i.e., $p_{\phi}(z_t|y, x_{\text{ref}})$. This significantly enhances stability during training and inference, as the model has a clearer target to optimize. Consequently, rather than randomly fluctuating among different interpretations of the prompt, the model can effectively concentrate its learning and sampling on the characteristics provided by x_{ref} .

4. Our Method

Based on the insight gained from mode analysis, we detail our method as follows. Starting with input prompt y , we generate a reference image x_{ref} using a pretrained text-to-image diffusion model. We then calculate the score $\nabla_{\theta}\mathcal{L}_{\text{ISD}}$ that utilizes both the text prompt and the image prompt for 3D optimization. To mitigate view bias by the reference image and the Janus problem, we incorporate additional multi-view regularization by jointly optimizing $\nabla_{\theta}\mathcal{L}_{\text{ISD}}$ with a multi-view prior $\nabla_{\theta}\mathcal{L}_{\text{SDS-MVD}}$. An overview of our method is shown in Figure 5.

4.1. Mode guidance using IP-Adapter

To implement mode guidance from a prior $p_{\phi}(z_t|y, x_{\text{ref}})$ with image prompt capability, we leverage IP-Adapter [61], a lightweight adapter model built upon a pretrained LDM model. To begin, we sample a reference image from an arbitrary text-to-image model, denoted as x_{ref} . Next, we extract a visual token of length L by passing x_{ref} through an image encoder. This encoder effectively transforms the visual information into a latent that can be utilized in conjunction with text prompt. The score distillation using the IP-adapter guidance can be formulated with the IP-SDS loss as:

$$\nabla_{\theta}\mathcal{L}_{\text{IP-SDS}} \triangleq \mathbb{E}_{t,\epsilon,c} \left[\omega(t) (\epsilon_{\text{IP}}(x_t, t, y, x_{\text{ref}}) - \epsilon) \frac{\partial g(\theta, c)}{\partial \theta} \right], \quad (4)$$

where ϵ_{IP} is the noise prediction using IP-adapter. As depicted in Fig. 2, by employing $p_{\phi}(z_t|y, x_{\text{ref}})$ as a teacher, the

visual information provided by x_{ref} guides the optimization to converge to a desirable mode, resulting in the improved 3D quality and training stability compared to the original SDS loss.

4.2. Improved control variates with IP-Adapter

An additional benefit of using IP-Adapter for mode guidance is that we can use it to build a strong control variate that further reduces variances in score estimates. Let us recall the derivative of the original SDS loss (see appendix A.4 of [38]). For SDS, the gradient can be derived from Eq. (1), which is equal to:

$$\mathbb{E}_{\epsilon} \left[\underbrace{\nabla_{\theta} \log q(z_t|\mathbf{x} = g(\theta))}_{(A)} - \underbrace{\nabla_{\theta} \log p_{\phi}(z_t|y)}_{(B)} \right], \quad (5)$$

where term (B) represents the score function estimated by the LDM’ Unet, while term (A) comprises two components – path derivatives and parameter score – that sum to zero, yielding the true gradient of SDS:

$$\nabla_{\theta}\mathcal{L}_{\text{SDS}} \triangleq \mathbb{E}_{t,\epsilon,c} \left[\omega(t) (\epsilon_{\theta}(x_t, t, y)) \frac{\partial g(\theta, c)}{\partial \theta} \right], \quad (6)$$

However, in practice, SDS chooses to keep the path derivative (ie. ϵ) and only discard the parameter score, as the path derivative can be positively correlated to other terms in (B). This leads to Eq. (2), where ϵ is the control variate for the prediction function. Here we introduce a reduced variance version of the gradient as follows:

$$\nabla_{\theta}\mathcal{L}_{\text{ISD}} \triangleq \mathbb{E}_{t,\epsilon,c} \left[\omega(t) \left(\epsilon_{\text{IP}}(x_t, t, y, x_{\text{ref}}) - \epsilon_{\text{SD}}(x_t, t, y) \right) \frac{\partial g(\theta, c)}{\partial \theta} \right], \quad (7)$$

which establishes our *image prompt score distillation* (ISD). The rationale behind ISD is that the noise prediction of the

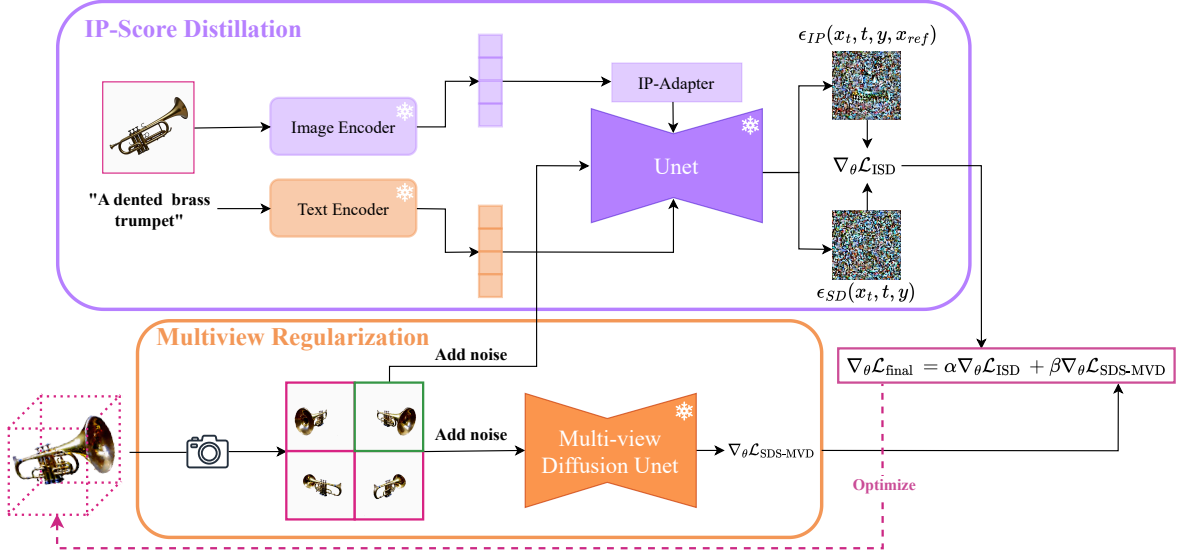


Figure 5. An overview of our method. Starting with input prompt y , we generate a reference image x_{ref} using a text-to-image model. Both the text prompt and the image prompt are used with the IP-Adapter for score distillation, following our ISD gradient $\nabla_{\theta} \mathcal{L}_{ISD}$. To mitigate view bias by reference image and the Janus problem, we incorporate additional multi-view regularization by jointly optimizing $\nabla_{\theta} \mathcal{L}_{ISD}$ with $\nabla_{\theta} \mathcal{L}_{SDS-MVD}$.

Unet without image prompt ϵ_{SD} can be closely aligned with those of the IP-Adapter since both still shares the same text prompt, which makes them correlate more positively than with a random noise estimate.

We found that the variance of the gradients is significantly reduced compared to the pure noise scenario as demonstrated in a 2D toy experiment for 10 prompts using IP-SDS, IP-VSD, and our proposed ISD method. The IP-VSD variant is the application of VSD loss [53] on the IP-Adapter prior instead of the original text-to-image prior. We recorded and calculated the gradient norm for each method, as shown in Fig. 3. Overall, the gradient norms of IP-VSD and IP-SDS display similar fluctuation patterns; however, IP-SDS exhibits less oscillation in the gradient norm, indicating that our approach more effectively controls SDS gradient variance when guided by the IP-Adapter. Remarkably, ISD yields results almost identical to IP-VSD in both 2D and 3D generations, as seen in Fig. 3 and Fig. 4. This finding suggests that, with the IP-Adapter as a teacher, the original Unet can effectively work as a control variate, eliminating the need for additional fine-tuning of the LoRA module in IP-VSD.

4.3. Multi-view regularization

A particular issue of using an image prompt to guide score distillation is that the model can be biased toward the reference image views, leading to the Janus problem in the output. To address this, we further leverage MVDream [46] as an additional multi-view regularization for score distillation

sampling:

$$\nabla_{\theta} \mathcal{L}_{SDS-MVD} \triangleq \mathbb{E}_{t, \epsilon, c} \left[\omega(t) (\epsilon_{MVD}(x_t, t, y) - \epsilon) \frac{\partial g(\theta, c)}{\partial \theta} \right], \quad (8)$$

where ϵ_{MVD} is the noise prediction of the MVDream model. Our combined score distillation is formulated as:

$$\nabla_{\theta} \mathcal{L}_{final} = \alpha \nabla_{\theta} \mathcal{L}_{ISD} + \beta \nabla_{\theta} \mathcal{L}_{SDS-MVD}, \quad (9)$$

where α and β are two scaling factors. During optimization, β gradually decreases to emphasize shape generation in the early iterations, while α gradually increases, shifting the focus toward texture rather than geometry as optimization progresses. The whole process is illustrated in Fig. 5. Both α and β are essential components of our methodology. If only α is provided, the resulting 3D outputs will be adversely affected by the Janus problem. Conversely, if only β is utilized, the generated 3D object will exhibit a smooth and toy-like texture, as illustrated in Fig. 6.

5. Experiments

Benchmark and metrics: We evaluate our method using T3bench [11], a benchmark that assesses both the quality and text prompt alignment of generated 3D models. T3bench consists of 300 prompts, categorized into three groups: single object, single object with surroundings, and multiple objects. For qualitative evaluation, T3bench converts a 3D representation into a mesh and defines a level-0 icosahedron, with vertices representing camera positions

Method	Time (mins)	Single Object			Single Object with Surr			Multiple Objects		
		Qual. \uparrow	Align. \uparrow	Avg \uparrow	Qual. \uparrow	Align. \uparrow	Avg \uparrow	Qual. \uparrow	Align. \uparrow	Avg \uparrow
Dreamfusion [38]	30	24.9	24.0	24.4	19.3	29.8	24.6	17.3	14.8	16.1
Magic3D [24]	40	38.7	35.3	37.0	29.8	41.0	35.4	26.6	24.8	25.7
LatentNeRF [35]	65	34.2	32.0	33.1	23.7	37.5	30.6	21.7	19.5	20.6
Fantasia3D [2]	45	29.2	23.5	26.4	21.9	32.0	27.0	22.7	14.3	18.5
SJC [51]	25	26.3	23.0	24.7	17.3	22.3	19.8	11.7	5.8	8.7
ProlificDreamer [53]	240	51.1	<u>47.8</u>	<u>49.4</u>	42.5	47.0	<u>44.8</u>	45.7	25.8	<u>35.8</u>
MVDream [46]	30	53.2	42.3	47.8	36.3	<u>48.5</u>	42.4	39.0	<u>28.5</u>	33.8
DreamGaussian [48]	7	19.9	19.8	19.8	10.4	17.8	14.1	12.3	9.5	10.9
GeoDream [32]	400	48.4	33.8	41.1	35.2	34.5	34.9	34.3	16.5	25.4
RichDreamer [39]	70	57.3	40.0	48.6	<u>43.9</u>	42.3	43.1	34.8	22.0	28.4
ISD (ours)	40	<u>55.4</u>	52.6	54.0	45.7	59.0	52.4	<u>43.4</u>	39.4	41.4

Table 1. Comparative results for the text-to-3D task across three settings of T3Bench. The best results are **bold** while the second best results are underlined.



Figure 6. Qualitative comparison between our approach and prior methods including MVDream, SDS, and VSD.



Figure 7. The effect of the IP scale indicates that as the IP scale increases, the generated 3D results align more closely with the reference image; however, this comes at the cost of worsening the Janus problem.

for multi-view image rendering. These images are processed by ImageReward [58], and the results are aggregated to generate a quality score. For text prompt alignment, each multi-view image is captioned using BLIP [21]. These cap-

tions, along with those of 3D models generated by CAP3D [31], are merged by ChatGPT and compared to the initial prompt.

IP Scale	Qual. \uparrow	Align. \uparrow
0.0	69.2	61.2
0.2	69.4	60.0
0.5	81.9	66.7
0.7	76.8	73.3
1.0	70.9	59.0

Table 2. Ablation study of different IP scales.

Control variate	Qual. \uparrow	Align. \uparrow
Rand. noise (CFG 7.5)	45.8	60.0
Rand. noise (CFG 100)	75.7	74.0
Unet LoRA	79.6	67.0
Unet ($t + \delta t$)	72.9	66.3
Unet (same t) (ours)	81.8	66.7

Table 3. Ablation study of different control variate elements.

Implementation details: Our method is implemented based on the ThreeStudio framework [9]. We train each 3D object for 6,000 iterations, using the IP-Adapter [61] version SD 1.5 as an approximation for $p_\phi(z_t|y, x_{\text{ref}})$, with the IP scale set to 0.5. We also employ MVDream [46] as a multi-view regularization technique to address the Janus problem. The scaling factors α and β in Eq. (9) are initially set to 0.4 and 0.6, respectively, with α increasing to 0.8 and β decreasing to 0.02 as training progresses. We employed a classifier-free guidance scale (CFG) of 7.5 for the ISD term and a CFG of 50 for the SDS-MVD regularization.

5.1. Comparison with prior methods

Quantitative Comparison: We use the methods presented in T3bench [11] as our comparison baseline, including DreamFusion [38], Magic3D [24], LatentNeRF [35], Fantasia3D [2], SJC [51], ProlificDreamer [53], MVDream [46], DreamGaussian [48], GeoDream [32], and RichDreamer [39]. Quantitative results are presented in Tab. 1. In the single-object category, our method achieves near SOTA performance, comparable to RichDreamer [39], while cutting training time nearly in half, surpassing previous methods. For single objects with surroundings, we attain the highest benchmark score. In the multiple-objects category, our method ranks second only to VSD, with a small margin, due to MVDream’s geometric limitations. However, by leveraging guidance from reference images, our method improves 3D model quality over raw MVDream [46]. Notably, our method achieves the highest alignment score across all categories due to effective reference image guidance.

Qualitative Comparison. We present comparisons with prior methods in Fig. 6. While SDS struggles with poor texture and geometry, VSD improves texture quality but still shows weak geometry. MVDream achieves reasonable geometry but suffers from toy-like textures due to its bias toward the Objaverse [5] dataset. In contrast, our method combines the strengths of both approaches, generating realistic geometry with MVDream’s constraints while achieving high-quality texture by leveraging the mode selected in the reference image.

5.2. Ablation study

In this section, we conduct several experiments to identify potential factors affecting our method, including the variance of the IP scale and various variance control strategies. We perform an ablation study using 20 prompts selected from three categories of the T3bench benchmark.

Effect of IP scale. Using IP-Adapter, the IP scale adjusts the influence of image prompting. We vary the IP scale across values [0.0, 0.2, 0.5, 0.7, 1.0] to evaluate its effect on our methods. Quantitative results are provided in Tab. 2, and qualitative results in Fig. 7. As shown, higher IP scales produce 3D objects that align more closely with the reference images but are also more prone to the Janus problem. We select an IP scale of 0.5 to balance reference image alignment with a reduced likelihood of the Janus problem.

Ablation of variate control. Another key factor in our method is the choice of control variate, represented by the second term in Eq. (7). In this study, we test several alternatives: replacing the Unet term with pure noise (IP-SDS), substituting Unet with a trainable LoRA (IP-VSD), and using Unet at $t + \delta t$ instead of time t . Both qualitative results in Fig. 4 and quantitative results in Tab. 3 show that using Unet as the control variate achieves results similar to Unet with LoRA, allowing our method to approximate IP-VSD without the additional LoRA training, thereby significantly speeding up training. Additionally, the Gaussian noise control variate requires a larger CFG value of 100 to yield coherent 3D objects, which notably raises the likelihood of the Janus problem. When using Unet at $t + \delta t$, the 3D quality is generally similar to that with our Unet at t , but some generated objects display missing components. Thus, we select Unet at t as our default control variate, achieving an effective balance of generation speed and 3D quality.

6. Limitations and Conclusion

Limitations: Although our method can generate high-quality 3D objects, it still suffers from the Janus problem due to biases in the views of the input images provided by the IP-Adapter. Additionally, our method is constrained by the performance of both the IP-Adapter and MVDream, which hinders its ability to generate composite objects. Another drawback is that the generated geometry may not always align with the reference image, resulting in significant geometric shifts in later iterations.

Conclusion: In this paper, we have introduced a novel framework for selecting a high-quality mode prior for text-to-3D generation. By leveraging the mode suggested by a reference image and a better control variate to reduce variance in score estimate, our method can generate high-quality 3D models at a reasonable speed. In future work, we aim to explore more effective mitigation strategies for the

Janus problem when utilizing the IP-Adapter as a mode selector. Additionally, we plan to extend our methods to various settings such as amortized optimization and for other 3D representations.

References

- [1] Anonymous. Eliminating oversaturation and artifacts of high guidance scales in diffusion models. In *Submitted to The Thirteenth International Conference on Learning Representations*, 2024. under review. 3
- [2] Rui Chen, Yongwei Chen, Ningxin Jiao, and Kui Jia. Fantasia3d: Disentangling geometry and appearance for high-quality text-to-3d content creation. In *Proceedings of the IEEE/CVF International Conference on Computer Vision (ICCV)*, 2023. 4, 7, 8, 2
- [3] Yang Chen, Yingwei Pan, Haibo Yang, Ting Yao, and Tao Mei. Vp3d: Unleashing 2d visual prompt for text-to-3d generation. In *CVPR*, 2024. 1, 4
- [4] Matt Deitke, Ruoshi Liu, Matthew Wallingford, Huong Ngo, Oscar Michel, Aditya Kusupati, Alan Fan, Christian Laforte, Vikram Voleti, Samir Yitzhak Gadre, Eli VanderBilt, Aniruddha Kembhavi, Carl Vondrick, Georgia Gkioxari, Kiana Ehsani, Ludwig Schmidt, and Ali Farhadi. Objaverse-xl: A universe of 10m+ 3d objects. *arXiv preprint arXiv:2307.05663*, 2023. 3
- [5] Matt Deitke, Dustin Schwenk, Jordi Salvador, Luca Weihs, Oscar Michel, Eli VanderBilt, Ludwig Schmidt, Kiana Ehsani, Aniruddha Kembhavi, and Ali Farhadi. Objaverse: A universe of annotated 3d objects. In *Proceedings of the IEEE/CVF Conference on Computer Vision and Pattern Recognition*, pages 13142–13153, 2023. 3, 8
- [6] Lihe Ding, Shaocong Dong, Zhanpeng Huang, Zibin Wang, Yiyuan Zhang, Kaixiong Gong, Dan Xu, and Tianfan Xue. Text-to-3d generation with bidirectional diffusion using both 2d and 3d priors. In *Proceedings of the IEEE/CVF Conference on Computer Vision and Pattern Recognition*, pages 5115–5124, 2024. 4
- [7] Patrick Esser, Sumith Kulal, Andreas Blattmann, Rahim Entezari, Jonas Müller, Harry Saini, Yam Levi, Dominik Lorenz, Axel Sauer, Frederic Boesel, et al. Scaling rectified flow transformers for high-resolution image synthesis. In *Forty-first International Conference on Machine Learning*, 2024. 1
- [8] Ian Goodfellow, Jean Pouget-Abadie, Mehdi Mirza, Bing Xu, David Warde-Farley, Sherjil Ozair, Aaron Courville, and Yoshua Bengio. Generative adversarial nets. *Advances in neural information processing systems*, 27, 2014. 3
- [9] Yuan-Chen Guo, Ying-Tian Liu, Ruizhi Shao, Christian Laforte, Vikram Voleti, Guan Luo, Chia-Hao Chen, Zi-Xin Zou, Chen Wang, Yan-Pei Cao, and Song-Hai Zhang. three-studio: A unified framework for 3d content generation, 2023. 8
- [10] Yuze He, Yushi Bai, Matthieu Lin, Wang Zhao, Yubin Hu, Jenny Sheng, Ran Yi, Juanzi Li, and Yong-Jin Liu. T³bench: Benchmarking current progress in text-to-3d generation, 2023. 2
- [11] Yuze He, Yushi Bai, Matthieu Lin, Wang Zhao, Yubin Hu, Jenny Sheng, Ran Yi, Juanzi Li, and Yong-Jin Liu. T³bench: Benchmarking current progress in text-to-3d generation, 2023. 1, 6, 8
- [12] Yicong Hong, Kai Zhang, Jiuxiang Gu, Sai Bi, Yang Zhou, Difan Liu, Feng Liu, Kalyan Sunkavalli, Trung Bui, and Hao Tan. LRM: Large reconstruction model for single image to 3d. In *The Twelfth International Conference on Learning Representations*, 2024. 3
- [13] Edward J Hu, Yelong Shen, Phillip Wallis, Zeyuan Allen-Zhu, Yuanzhi Li, Shean Wang, Lu Wang, and Weizhu Chen. LoRA: Low-rank adaptation of large language models. In *International Conference on Learning Representations*, 2022. 4
- [14] Yukun Huang, Jianan Wang, Yukai Shi, Boshi Tang, Xianbiao Qi, and Lei Zhang. Dreamtime: An improved optimization strategy for diffusion-guided 3d generation. In *The Twelfth International Conference on Learning Representations*, 2024. 4
- [15] Ajay Jain, Ben Mildenhall, Jonathan T Barron, Pieter Abbeel, and Ben Poole. Zero-shot text-guided object generation with dream fields. In *Proceedings of the IEEE/CVF Conference on Computer Vision and Pattern Recognition*, pages 867–876, 2022. 3
- [16] Chenhan Jiang, Yihan Zeng, Tianyang Hu, Songcun Xu, Wei Zhang, Hang Xu, and Dit-Yan Yeung. Jointdreamer: Ensuring geometry consistency and text congruence in text-to-3d generation via joint score distillation. In *European Conference on Computer Vision*, pages 439–456. Springer, 2025. 4
- [17] Heewoo Jun and Alex Nichol. Shap-e: Generating conditional 3d implicit functions, 2023. 2
- [18] Oren Katzir, Or Patashnik, Daniel Cohen-Or, and Dani Lischinski. Noise-free score distillation. In *The Twelfth International Conference on Learning Representations*, 2024. 4
- [19] Bernhard Kerbl, Georgios Kopanas, Thomas Leimkühler, and George Drettakis. 3d gaussian splatting for real-time radiance field rendering. *ACM Transactions on Graphics*, 42 (4), 2023. 1, 4
- [20] Kyungmin Lee, Kihyuk Sohn, and Jinwoo Shin. Dreamflow: High-quality text-to-3d generation by approximating probability flow. In *The Twelfth International Conference on Learning Representations*, 2024. 4
- [21] Junnan Li, Dongxu Li, Caiming Xiong, and Steven Hoi. Blip: Bootstrapping language-image pre-training for unified vision-language understanding and generation. In *ICML*, 2022. 7
- [22] Jiahao Li, Hao Tan, Kai Zhang, Zexiang Xu, Fujun Luan, Yinghao Xu, Yicong Hong, Kalyan Sunkavalli, Greg Shakhnarovich, and Sai Bi. Instant3d: Fast text-to-3d with sparse-view generation and large reconstruction model. In *The Twelfth International Conference on Learning Representations*, 2024. 3, 2
- [23] Wei Yu Li, Jiarui Liu, Rui Chen, Yixun Liang, Xuelin Chen, Ping Tan, and Xiaoxiao Long. Craftsman: High-fidelity mesh generation with 3d native generation and interactive geometry refiner. *arXiv preprint arXiv:2405.14979*, 2024. 3

- [24] Chen-Hsuan Lin, Jun Gao, Luming Tang, Towaki Takikawa, Xiaohui Zeng, Xun Huang, Karsten Kreis, Sanja Fidler, Ming-Yu Liu, and Tsung-Yi Lin. Magic3d: High-resolution text-to-3d content creation. In *IEEE Conference on Computer Vision and Pattern Recognition (CVPR)*, 2023. 1, 4, 7, 8, 2
- [25] Minghua Liu, Chao Xu, Haian Jin, Linghao Chen, Mukund Varma T, Zexiang Xu, and Hao Su. One-2-3-45: Any single image to 3d mesh in 45 seconds without per-shape optimization. In *Thirty-seventh Conference on Neural Information Processing Systems*, 2023. 2
- [26] Minghua Liu, Chao Xu, Haian Jin, Linghao Chen, Mukund Varma T, Zexiang Xu, and Hao Su. One-2-3-45: Any single image to 3d mesh in 45 seconds without per-shape optimization. *Advances in Neural Information Processing Systems*, 36, 2024. 3
- [27] Qiang Liu and Dilin Wang. Stein variational gradient descent: A general purpose bayesian inference algorithm. *Advances in neural information processing systems*, 29, 2016. 1
- [28] Ruoshi Liu, Rundi Wu, Basile Van Hoorick, Pavel Tokmakov, Sergey Zakharov, and Carl Vondrick. Zero-1-to-3: Zero-shot one image to 3d object. In *Proceedings of the IEEE/CVF International Conference on Computer Vision (ICCV)*, pages 9298–9309, 2023. 2, 3, 4
- [29] Yuan Liu, Cheng Lin, Zijiao Zeng, Xiaoxiao Long, Lingjie Liu, Taku Komura, and Wenping Wang. Syncdreamer: Generating multiview-consistent images from a single-view image. In *The Twelfth International Conference on Learning Representations*, 2024. 3
- [30] Jonathan Lorraine, Kevin Xie, Xiaohui Zeng, Chen-Hsuan Lin, Towaki Takikawa, Nicholas Sharp, Tsung-Yi Lin, Ming-Yu Liu, Sanja Fidler, and James Lucas. Att3d: Amortized text-to-3d object synthesis. *The International Conference on Computer Vision (ICCV)*, 2023. 4
- [31] Tiange Luo, Chris Rockwell, Honglak Lee, and Justin Johnson. Scalable 3d captioning with pretrained models. In *Advances in Neural Information Processing Systems*, pages 75307–75337. Curran Associates, Inc., 2023. 7
- [32] Baorui Ma, Haoge Deng, Junsheng Zhou, Yu-Shen Liu, Tiejun Huang, and Xinlong Wang. Geodream: Disentangling 2d and geometric priors for high-fidelity and consistent 3d generation. *arXiv preprint arXiv:2311.17971*, 2023. 1, 3, 4, 7, 8
- [33] Zhiyuan Ma, Yuxiang Wei, Yabin Zhang, Xiangyu Zhu, Zhen Lei, and Lei Zhang. Scaledreamer: Scalable text-to-3d synthesis with asynchronous score distillation. *The 18th European Conference on Computer Vision (ECCV)*, 2024. 3, 4, 5
- [34] Luke Melas-Kyriazi, Iro Laina, Christian Rupprecht, and Andrea Vedaldi. Realfusion: 360deg reconstruction of any object from a single image. In *Proceedings of the IEEE/CVF Conference on Computer Vision and Pattern Recognition (CVPR)*, pages 8446–8455, 2023. 3
- [35] Gal Metzer, Elad Richardson, Or Patashnik, Raja Giryes, and Daniel Cohen-Or. Latent-nerf for shape-guided generation of 3d shapes and textures. In *Proceedings of the IEEE/CVF Conference on Computer Vision and Pattern Recognition (CVPR)*, pages 12663–12673, 2023. 1, 4, 7, 8, 2
- [36] Ben Mildenhall, Pratul P. Srinivasan, Matthew Tancik, Jonathan T. Barron, Ravi Ramamoorthi, and Ren Ng. Nerf: Representing scenes as neural radiance fields for view synthesis. In *ECCV*, 2020. 1, 4
- [37] Alex Nichol, Heewoo Jun, Pratul Dhariwal, Pamela Mishkin, and Mark Chen. Point-e: A system for generating 3d point clouds from complex prompts, 2022. 2
- [38] Ben Poole, Ajay Jain, Jonathan T. Barron, and Ben Mildenhall. Dreamfusion: Text-to-3d using 2d diffusion. In *The Eleventh International Conference on Learning Representations*, 2023. 1, 3, 4, 5, 7, 8, 2
- [39] Lingteng Qiu, Guanying Chen, Xiaodong Gu, Qi Zuo, Mutian Xu, Yushuang Wu, Weihao Yuan, Zilong Dong, Liefeng Bo, and Xiaoguang Han. Richdreamer: A generalizable normal-depth diffusion model for detail richness in text-to-3d. In *Proceedings of the IEEE/CVF Conference on Computer Vision and Pattern Recognition*, pages 9914–9925, 2024. 1, 3, 4, 7, 8, 2
- [40] Aditya Ramesh, Mikhail Pavlov, Gabriel Goh, Scott Gray, Chelsea Voss, Alec Radford, Mark Chen, and Ilya Sutskever. Zero-shot text-to-image generation. In *Proceedings of the 38th International Conference on Machine Learning*, pages 8821–8831. PMLR, 2021. 3
- [41] Robin Rombach, Andreas Blattmann, Dominik Lorenz, Patrick Esser, and Björn Ommer. High-resolution image synthesis with latent diffusion models. In *CVPR*, 2022. 1
- [42] Chitwan Saharia, William Chan, Saurabh Saxena, Lala Li, Jay Whang, Emily Denton, Seyed Kamyar Seyed Ghasemipour, Raphael Gontijo-Lopes, Burcu Karagol Ayan, Tim Salimans, Jonathan Ho, David J. Fleet, and Mohammad Norouzi. Photorealistic text-to-image diffusion models with deep language understanding. In *Advances in Neural Information Processing Systems*, 2022. 3
- [43] Christoph Schuhmann, Romain Beaumont, Richard Vencu, Cade Gordon, Ross Wightman, Mehdi Cherti, Theo Coombes, Aarush Katta, Clayton Mullis, Mitchell Wortsman, Patrick Schramowski, Srivatsa Kundurthy, Katherine Crowson, Ludwig Schmidt, Robert Kaczmarczyk, and Jenia Jitsev. Laion-5b: An open large-scale dataset for training next generation image-text models, 2022. 3
- [44] Qiuhong Shen, Zike Wu, Xuanyu Yi, Pan Zhou, Hanwang Zhang, Shuicheng Yan, and Xinchao Wang. Gamba: Marry gaussian splatting with mamba for single view 3d reconstruction. *arXiv preprint arXiv:2403.18795*, 2024. 3
- [45] Ruoxi Shi, Hansheng Chen, Zhuoyang Zhang, Minghua Liu, Chao Xu, Xinyue Wei, Linghao Chen, Chong Zeng, and Hao Su. Zero123++: a single image to consistent multi-view diffusion base model, 2023. 2, 3
- [46] Yichun Shi, Peng Wang, Jianglong Ye, Long Mai, Kejie Li, and Xiao Yang. MVDream: Multi-view diffusion for 3d generation. In *The Twelfth International Conference on Learning Representations*, 2024. 2, 3, 6, 7, 8
- [47] Jiayang Tang, Zhaoxi Chen, Xiaokang Chen, Tengfei Wang, Gang Zeng, and Ziwei Liu. Lgm: Large multi-view gaussian model for high-resolution 3d content creation, 2024. 3

- [48] Jiaxiang Tang, Jiawei Ren, Hang Zhou, Ziwei Liu, and Gang Zeng. Dreamgaussian: Generative gaussian splatting for efficient 3d content creation. In *The Twelfth International Conference on Learning Representations*, 2024. 4, 7, 8, 2
- [49] Dmitry Tochilkin, David Pankratz, Zexiang Liu, Zixuan Huang, , Adam Letts, Yangguang Li, Ding Liang, Christian Laforte, Varun Jampani, and Yan-Pei Cao. Tripotr: Fast 3d object reconstruction from a single image. *arXiv preprint arXiv:2403.02151*, 2024. 3
- [50] Uy Dieu Tran, Minh Luu, Phong Ha Nguyen, Khoi Nguyen, and Binh-Son Hua. Diverse text-to-3d synthesis with augmented text embedding. In *Proceedings of the European Conference on Computer Vision*, 2024. 4, 1
- [51] Haochen Wang, Xiaodan Du, Jiahao Li, Raymond A. Yeh, and Greg Shakhnarovich. Score jacobian chaining: Lifting pretrained 2d diffusion models for 3d generation. In *Proceedings of the IEEE/CVF Conference on Computer Vision and Pattern Recognition (CVPR)*, pages 12619–12629, 2023. 7, 8, 2
- [52] Peng Wang and Yichun Shi. Imagedream: Image-prompt multi-view diffusion for 3d generation. *arXiv preprint arXiv:2312.02201*, 2023. 3
- [53] Zhengyi Wang, Cheng Lu, Yikai Wang, Fan Bao, Chongxuan Li, Hang Su, and Jun Zhu. Prolificdreamer: High-fidelity and diverse text-to-3d generation with variational score distillation. *NeurIPS*, 2023. 1, 3, 4, 5, 6, 7, 8, 2
- [54] Zhengyi Wang, Yikai Wang, Yifei Chen, Chendong Xiang, Shuo Chen, Dajiang Yu, Chongxuan Li, Hang Su, and Jun Zhu. Crm: Single image to 3d textured mesh with convolutional reconstruction model. In *European Conference on Computer Vision*, pages 57–74. Springer, 2025. 3
- [55] Haohan Weng, Tianyu Yang, Jianan Wang, Yu Li, Tong Zhang, CL Chen, and Lei Zhang. Consistent123: Improve consistency for one image to 3d object synthesis. *arXiv preprint arXiv:2310.08092*, 2023. 3
- [56] Tong Wu, Guandao Yang, Zhibing Li, Kai Zhang, Ziwei Liu, Leonidas Guibas, Dahua Lin, and Gordon Wetzstein. Gpt-4v(ision) is a human-aligned evaluator for text-to-3d generation. In *CVPR*, 2024. 1, 2
- [57] Kevin Xie, Jonathan Lorraine, Tianshi Cao, Jun Gao, James Lucas, Antonio Torralba, Sanja Fidler, and Xiaohui Zeng. Latte3d: Large-scale amortized text-to-enhanced3d synthesis. *The 18th European Conference on Computer Vision (ECCV)*, 2024. 3
- [58] Jiazheng Xu, Xiao Liu, Yuchen Wu, Yuxuan Tong, Qinkai Li, Ming Ding, Jie Tang, and Yuxiao Dong. Imagereward: Learning and evaluating human preferences for text-to-image generation. In *Advances in Neural Information Processing Systems*, pages 15903–15935. Curran Associates, Inc., 2023. 7
- [59] Jiale Xu, Weihao Cheng, Yiming Gao, Xintao Wang, Shenghua Gao, and Ying Shan. Instantmesh: Efficient 3d mesh generation from a single image with sparse-view large reconstruction models. *arXiv preprint arXiv:2404.07191*, 2024. 3
- [60] Runjie Yan, Kailu Wu, and Kaisheng Ma. Flow score distillation for diverse text-to-3d generation. *arXiv preprint arXiv:2405.10988*, 2024. 4
- [61] Hu Ye, Jun Zhang, Sibio Liu, Xiao Han, and Wei Yang. Ip-adaptor: Text compatible image prompt adapter for text-to-image diffusion models. *arXiv preprint arXiv:2308.06721*, 2023. 1, 2, 3, 5, 8
- [62] Taoran Yi, Jiemin Fang, Junjie Wang, Guanjun Wu, Lingxi Xie, Xiaopeng Zhang, Wenyu Liu, Qi Tian, and Xinggang Wang. Gaussiandreamer: Fast generation from text to 3d gaussians by bridging 2d and 3d diffusion models. In *CVPR*, 2024. 4
- [63] Jiahui Yu, Yuanzhong Xu, Jing Yu Koh, Thang Luong, Gunjan Baid, Zirui Wang, Vijay Vasudevan, Alexander Ku, Yinfei Yang, Burcu Karagol Ayan, Ben Hutchinson, Wei Han, Zarana Parekh, Xin Li, Han Zhang, Jason Baldridge, and Yonghui Wu. Scaling autoregressive models for content-rich text-to-image generation. *Transactions on Machine Learning Research*, 2022. 3
- [64] Xin Yu, Yuan-Chen Guo, Yangguang Li, Ding Liang, Song-Hai Zhang, and Xiaojuan Qi. Text-to-3d with classifier score distillation. In *The Twelfth International Conference on Learning Representations*, 2024. 4
- [65] Xin Yu, Yuan-Chen Guo, Yangguang Li, Ding Liang, Song-Hai Zhang, and Xiaojuan Qi. Text-to-3d with classifier score distillation. In *The Twelfth International Conference on Learning Representations*, 2024. 4
- [66] Kai Zhang, Sai Bi, Hao Tan, Yuanbo Xiangli, Nanxuan Zhao, Kalyan Sunkavalli, and Zexiang Xu. Gs-lrm: Large reconstruction model for 3d gaussian splatting. *European Conference on Computer Vision*, 2024. 3

ModeDreamer: Mode Guiding Score Distillation for Text-to-3D Generation using Reference Image Prompts

Supplementary Material

In this supplementary material, we provide additional evaluations of our method. Sec. 1 includes a quantitative assessment using GPTEval3D [56], a human-aligned evaluator for text-to-3D generation. Sec. 2 presents more qualitative results of the generated 3D models including results with 3DGS, diverse results with the same prompts provided different reference images, and more qualitative results.

1. Evaluation with GPTEval3D

We provide an additional assessment of our methods using GPTEval3D [56], a human-aligned evaluator for text-to-3D generation. Specifically, GPTEval3D evaluates the quality of 3D objects over 110 prompts across five criteria: Text-Asset Alignment, 3D Plausibility, Text-Geometry Alignment, Texture Details, and Geometry Details. For each evaluation, a pair of objects generated by two different methods, along with an input prompt and an evaluation criterion, is submitted to a large language model (e.g., GPT), which outputs its preference for one object over the other. This process is analogous to a user study but conducted by a large language model. The scores are aggregated to calculate an Elo score, with higher scores indicating better performance in the respective criteria [56].

The quantitative results are presented in Tab. 4. Our methods achieve the highest overall score and maintain superior performance in four out of five criteria, except Text-Asset Alignment, where our method is ranked second to RichDreamer [39]. These quantitative results, along with those provided by T3Bench [11] (Tab. 1 main paper), demonstrate that our method can generate high-quality 3D objects with strong text alignment.

2. More Qualitative Results

Qualitative results with 3DGS. We further demonstrate the effectiveness of our method by optimizing a 3D Gaussian splatting (3DGS) representation [19]. Our results are shown in Fig. 8, demonstrating that our method generalizes effectively to different 3D representations, including NeRFs and 3DGS.

Diversity results. We further evaluate the diversity of our 3D generation by considering various reference images sampled with the same prompts. As shown in Fig. 9, each reference image leads to distinct 3D results. Another approach that enhances the diversity of the text-to-3D task is DiverseDream [50], which utilizes the structure of reference images by employing textual inversion to diversify

the generated 3D objects. However, this method is unstable and struggles to generate asymmetric 3D objects, primarily due to overfitting issues associated with the textual inversion stage. In contrast, our proposed method is able to generate high-quality and diverse 3D objects while preserving reasonable geometric integrity. Furthermore, our results better align with the input references compared to DiverseDream [50], as illustrated in Fig. 10.

Additional qualitative results. Finally, we present additional qualitative results in Fig. 11, Fig. 12 and Fig. 13. Specifically, we use prompts from two benchmarks, T3Bench and GPTEval3D, along with additional prompts sourced from DreamFusion [38].

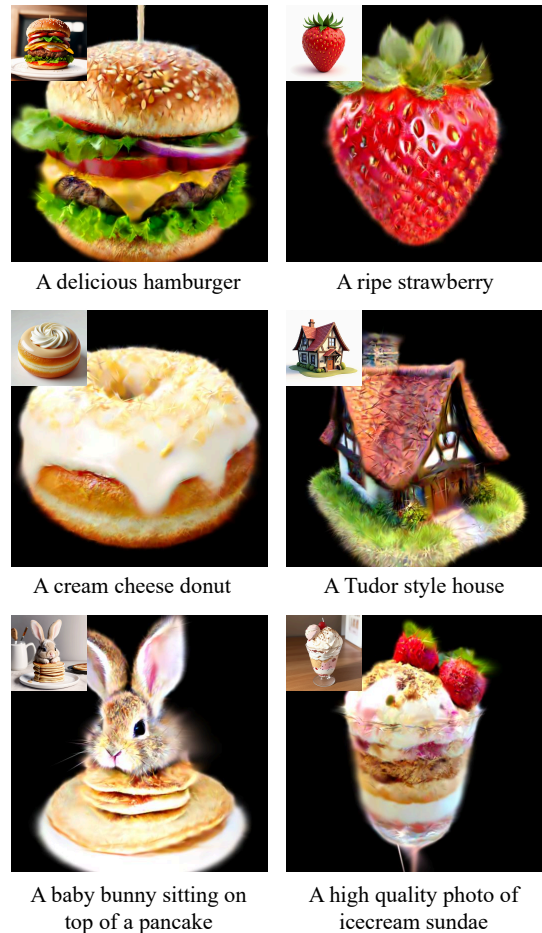


Figure 8. Qualitative results with 3D Gaussian splatting.

Methods	Text-Asset Alignment \uparrow	3D Plausi- bility \uparrow	Text-Geometry Alignment \uparrow	Texture Details \uparrow	Geometry Details \uparrow	Overall \uparrow
RichDreamer [39]	1295	<u>1225</u>	<u>1260</u>	<u>1356</u>	1251	<u>1277</u>
MVDream [46]	1271	1147	1251	1325	<u>1255</u>	1250
ProlificDreamer [53]	1262	1059	1152	1246	1181	1180
LatentNeRF [35]	1222	1145	1157	1180	1161	1173
Instant3D [22]	1200	1088	1153	1152	1181	1155
Magic3D [24]	1152	1001	1084	1178	1100	1100
DreamGaussian [48]	1101	954	1159	1126	1131	1094
SJC [51]	1130	995	1034	1080	1043	1056
Fantasia3D [2]	1068	892	1006	1109	1027	1021
Dreamfusion [38]	1000	1000	1000	1000	1000	1000
One2345 [25]	872	829	850	911	860	864
Shap-E [17]	843	842	846	784	846	836
Point-E [37]	725	690	689	716	746	713
ISD (ours)	<u>1291</u>	1271	1269	1370	1266	1294

Table 4. Comparison with text-to-3D methods using GPTEval3D [56] benchmark. The best results are bold while the second best results are underlined.

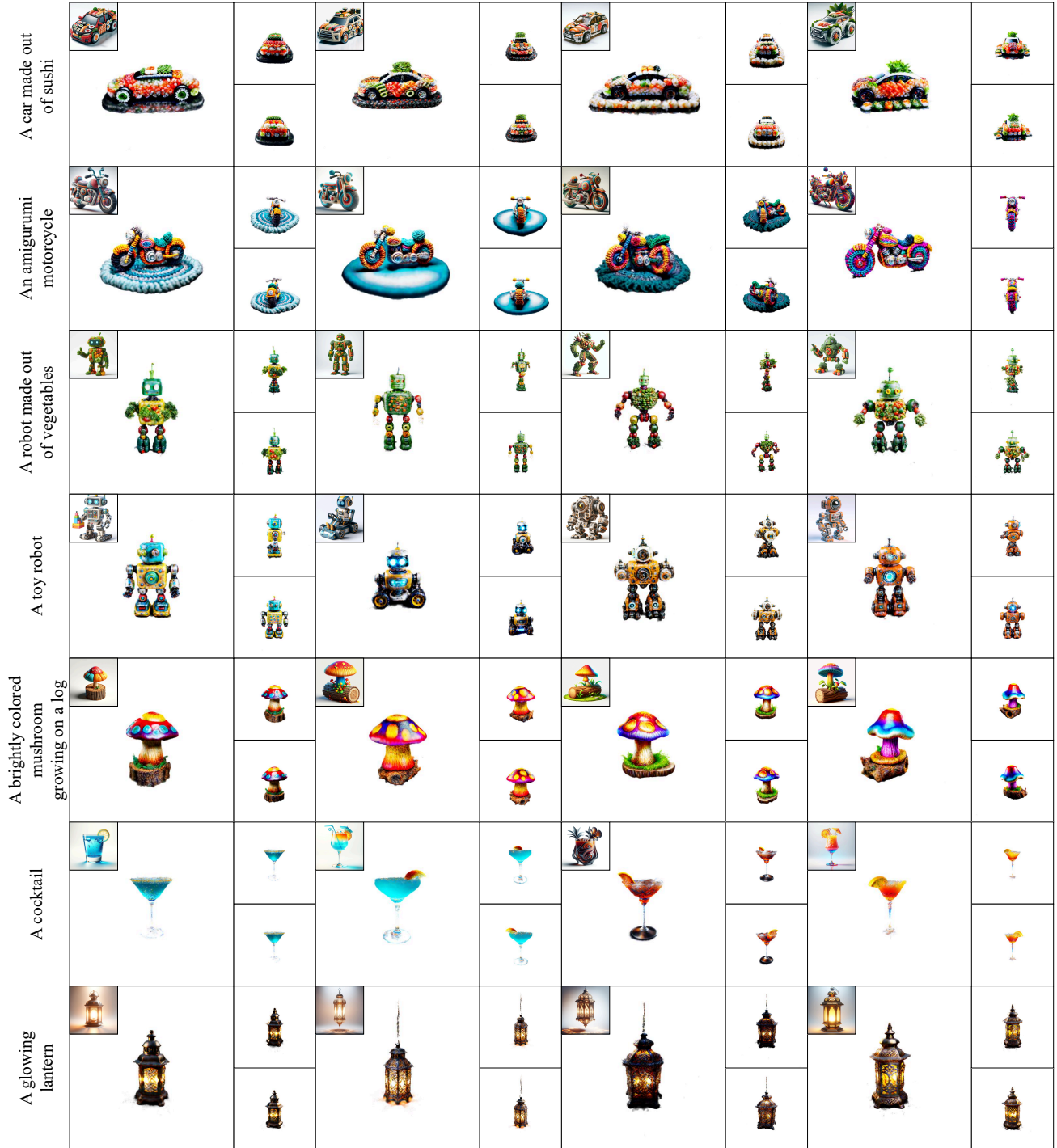


Figure 9. Diverse results of our method when varying the input reference images for each text prompt.



Figure 10. Diverse results of our method when comparing with DiverseDream [50]

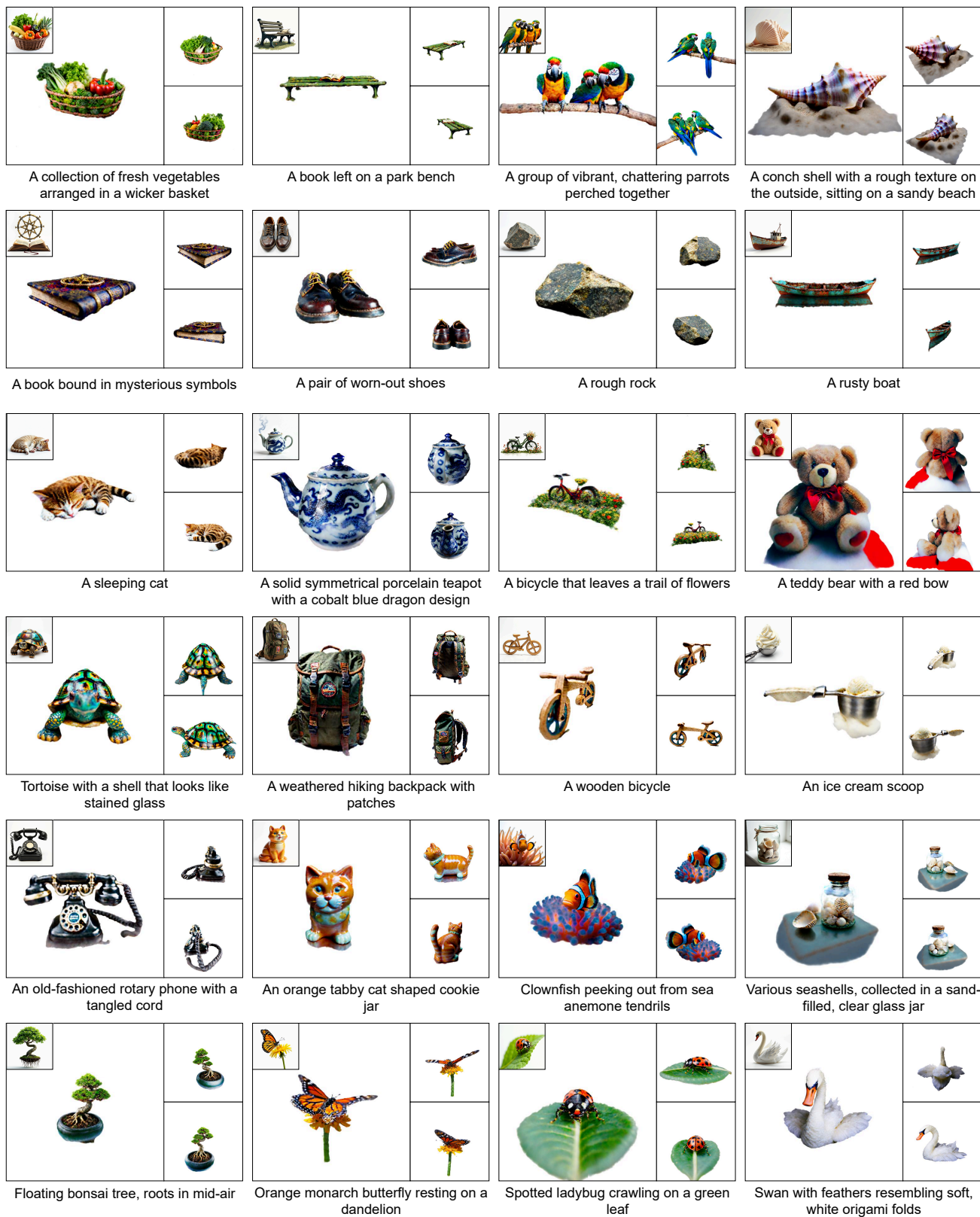


Figure 11. Additional qualitative results (1/3).

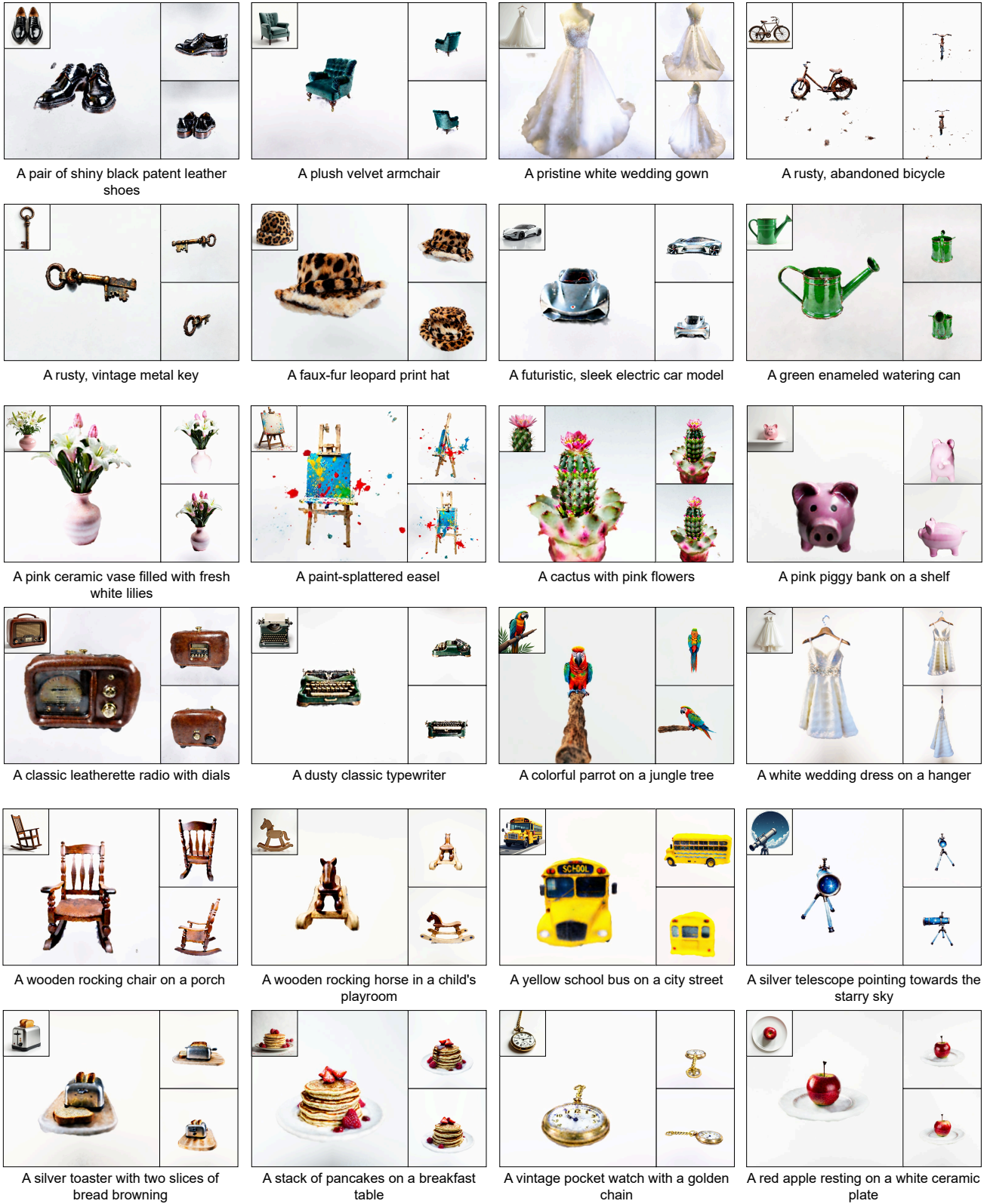
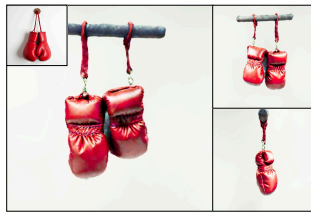


Figure 12. Additional qualitative results (2/3).



A pair of red boxing gloves hanging on a wall



A red rose in a crystal vase



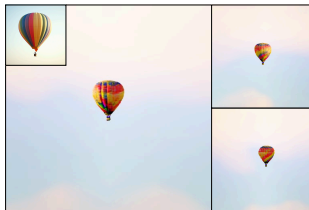
A silver teapot on a dining table



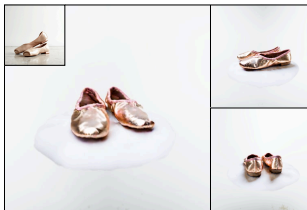
A pair of hiking boots on a trail



A delicate china teacup resting on a lace doily



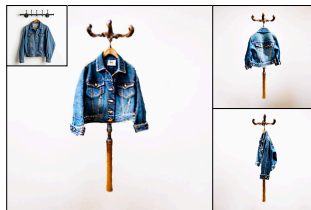
A hot air balloon in a clear sky



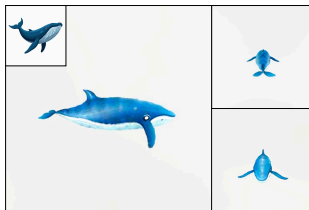
A pair of ballet shoes on a dance floor



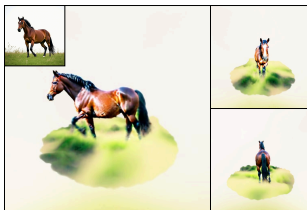
A black grand piano in a concert hall



A blue denim jacket hanging on a metal coat rack



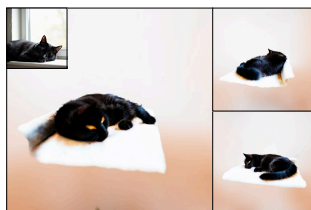
A blue whale in the deep ocean



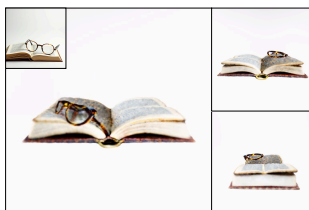
A brown horse in a green pasture



A chocolate cake on a white plate



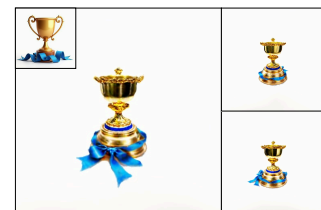
A black cat sleeping on a windowsill



An open book sits beside a vintage brass spectacles



A pizza is cooling beside a half-drunk can of soda



A golden trophy shines brightly next to a ruffled blue ribbon



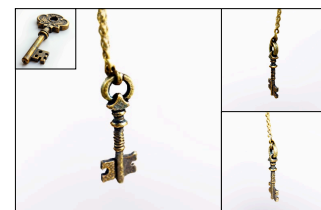
A woolen knitted scarf is wrapped around a pumpkin



An clock and a retro radio on the dusty shelf



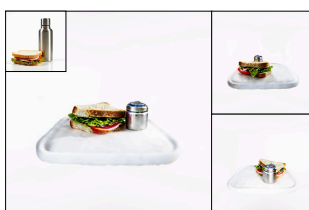
An apple lays nestled next to a vintage pocket watch



An old brass key



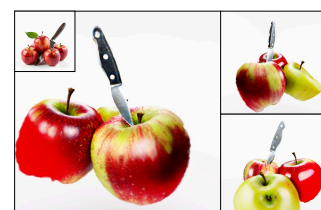
A glowing lantern rests beside a paperback book



A half-eaten sandwich sits next to a lukewarm thermos



A black cat sleeps peacefully beside a carved pumpkin



Ripe apples cluster next to a gleaming knife

Figure 13. Additional qualitative results (3/3).